IMAGING AND ANALYSIS OF PRE-BREAKDOWN SITES IN MULTICRYSTALLINE SILICON SOLAR CELLS

K. Bothe[1,a)], D. Hinken[1], K. Ramspeck[1,b)], S. Herlufsen[1], J. Schmidt[1], R. Brendel[1],
J. Bauer[2], J.-M. Wagner[2], N. Zakharov[2], and O. Breitenstein[2]
[1]Institut für Solarenergieforschung Hameln (ISFH), Am Ohrberg 1, D-31860 Emmerthal, Germany
[2]Max Planck Institute of Microstructure Physics, Weinberg 2, D-06120 Halle, Germany

ABSTRACT: We report on studies of the emission of light from industrial multicrystalline silicon solar cells under forward and reverse bias. Camera-based luminescence and dark lock-in thermography imaging techniques are used to study the spatial distribution of and energy dissipation at pre-breakdown sites. The pre-breakdown is associated with an increase in temperature and the emission of visible light. Three different breakdown types are distinguished by investigating the local luminescence and dark lock-in thermography signal as a function of the reverse bias. Moreover, we show that specific areas characterized by recombination active fine dendritic lines also give rise to sub-band-gap luminescence. This luminescence has a broad wavelength distribution with a maximum at around 1550 nm. Studies of multicrystalline silicon solar cells with different interstitial oxygen concentrations and electron microscopic analysis suggest that this light emission is directly related to clusters of oxygen.
Keywords: luminescence, imaging, thermography, multicrystalline, silicon

1 INTRODUCTION

The breakdown voltage of a solar cell is an important parameter for its classification. In case one silicon solar cell in a string of a solar module is shadowed or partly broken, this cell is reverse biased by the other cells in that string to about 10 to 20 V. Thus, the breakdown voltage of a solar cell should be considerably higher. Assuming an ideal abrupt junction and a base doping concentration between 5×10^{15} and 1×10^{16} cm^{-3} one would expect a breakdown voltage in the range of 90 to 60 V [1]. However, especially in mc-Si solar cells breakdown is often observed at considerably lower voltages and predominantly occurs at localized spots. Large current flows through these pre-breakdown sites result in the formation of so-called micro plasmas which are accompanied by the emission of visible light in the wavelength range between 500 and 1000 nm [2-5]. At the same time the current flow also results in local heating [6]. In photovoltaic modules, the temperature of those *hot spots* might become high enough to cause a damage of the module encapsulation. Using infrared imaging hot spots have been found to occur preferentially in dislocation-rich areas [7]. Interestingly, luminescence emission in the wavelength range between 1500 and 1700 nm, resulting from radiative recombination via defect states in the band gap, is also primarily found in areas of high dislocation density [8]. In this work we address the question whether the physical origin of the sub-band-gap luminescence and the local pre-breakdown is the same.

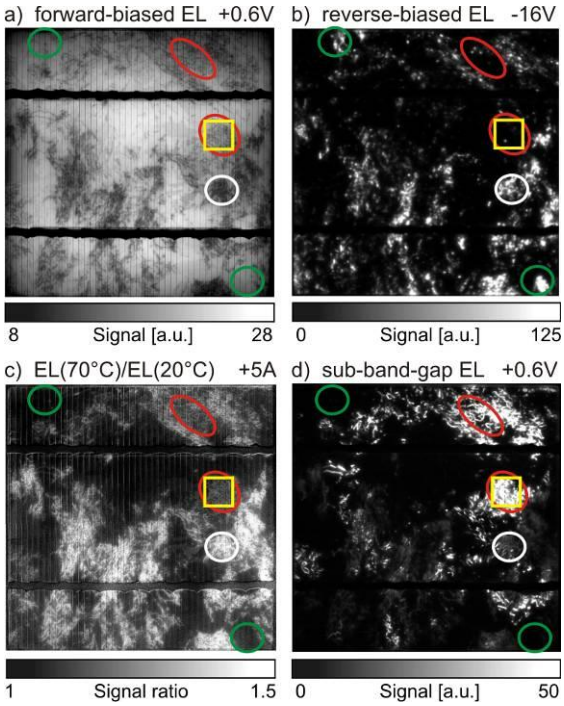

Figure 1: Electroluminescence images captured under different bias conditions and sample temperatures. a) EL image at 0.6 V forward bias, b) luminescence emission image under -16 V reverse bias, c) ratio image of two EL images captured under the same current conditions of 5 A at T=70 and 20°C, d) integral (1450 to 1700 nm) sub-band-gap luminescence at 0.6 V forward bias,

2 EXPERIMENTAL RESULTS

2.1 Setup and measurement details

The experimental setup consists of a blackened box which is equipped with either of two cameras. While for the luminescence imaging a 640×512 pixel focal plane array InGaAs camera is used, the DLIT measurements are performed using an infrared camera with an MCT sensor sensitive in the wavelength range from 3.9 to 5 µm. For both measurements the solar cells are connected to a bipolar power source using a four-point contacting scheme with 25 probes on each bus bar. During the measurements, a thermostat stabilizes the temperature of the solar cell at 25 °C. The DLIT measurements are performed at a lock-in frequency of 20 Hz corresponding to a thermal diffusion length of 1.2 mm in silicon. All electrolumines-

a) Electronic mail: k.bothe@isfh.de
b) Present address: SCHOTT Solar AG, Carl-Zeiss-Str. 4m D-63755 Alzenau, Germany

cence (EL) images are corrected for stray light and dark noise by subtracting a dark image recorded at equal exposure time but with no voltage applied to the cell under test. Detailed descriptions of the physical principles underlying the camera-based DLIT and EL techniques can be found elsewhere [9-13]. TEM images were taken with a Philips CM 20 TWIN TEM which is equipped with an EDX analysis system by Noran Instruments. The samples under test are 125×125 mm^2 alkaline-textured industrial multicrystalline silicon solar cells.

2.2 Results and discussion

Figure 1 shows luminescence emission images of a block-cast multi-crystalline silicon solar cell under forward and reverse bias. In image a) of Fig. 1 the band-to-band luminescence emission under 0.6 V forward bias is shown. This EL image shows areas of strongly reduced EL signal along fine dendritic lines (areas marked red) as well as areas with an even higher density of recombination active sites appearing as dark clusters (area marked white). The dendritic lines are typical for multicrystalline silicon and originate from intra-grain defects such as stacking faults and dislocations. These crystallographic defects are often decorated by impurities or impurity clusters and give rise to an increased non-radiative recombination activity and thus to a decreased EL signal. In those regions appearing as dark clusters the density of recombination active sites is considerably enhanced such that dendritic lines can hardly be recognized and it remains unclear whether only the density of dendritic lines is so much higher in these areas or if additional recombination sites are responsible for the low EL signal.

Fig. 1 b) shows the light emission image at -16 V reverse bias. The light emission in the reverse-EL mode is related to local avalanche breakdown [14,15] or internal field emission (IFE) [16] accompanied by the emission of light [17,18]. However, more complex mechanisms like impact ionization of deep states [19,20] and trap-assisted tunneling might also be responsible for the light emission. In regions appearing as dark clusters in the EL image under forward bias (compare e.g. areas marked white in Fig. 1 a) and 1 b)) we also detect breakdown-related light emission under reverse bias. As can be seen from Fig. 1c), for both regions appearing dark in the EL image we find a strong change of the EL signal with temperature indicating a strong temperature dependence of the carrier lifetime. In the cluster type regions the change with temperature is found to be stronger compared to dendritic line type regions.

Fig. 1 d) shows the sub-band-gap luminescence image for the wavelength range between 1450 and 1700 nm at 0.6 V forward bias. Comparing images a), b) and c) of Fig. 1 and especially those areas marked red, it becomes obvious that **sub-band-gap luminescence predominantly occurs in regions characterized by dendritic lines in the EL image** and that **breakdown-related emission under reverse bias is *not* observed in these regions**. These results confirm previous results by Kasemann et al.[21] obtained for similar samples using the same characterization techniques.

In conclusion, areas exist where sub-band-gap luminescence is found *independent* of the occurrence of breakdown-related luminescence even though a broad distribution of energy states is a preferential situation for trap-assisted tunneling under reverse bias. Thus, on the microscopic scale the origin of sub-band-gap luminescence under forward bias and breakdown-related luminescence emission under reverse bias **must** be different.

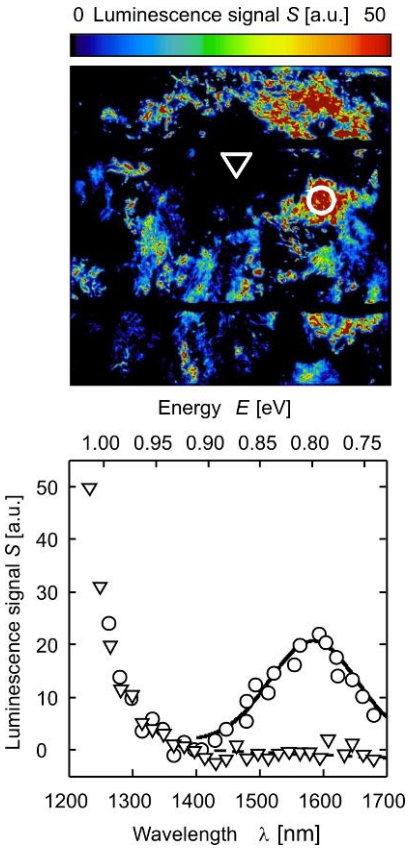

Figure 2: Upper: image of the integral luminescence emission in the wavelength range between 1450 to 1700 nm of a multicrystalline silicon solar cell (same cell as in Fig. 2) detected at 0.6 V forward bias using an InGaAs camera; Lower: luminescence spectrum of a representative area showing a high sub-band-gap luminescence in comparison with an area showing no sub-band gap luminescence.

As shown in Fig. 2, a spectral analysis of the sub-band-gap luminescence reveals a broad peak with a maximum at around 1550 nm indicating a rather broad distribution of energy states with a maximum located at around 0.8 eV away from the conduction or valence band. Similar spectra have previously been published by Tajima [22] attributing their occurrence to oxygen clusters formed during annealing of Czochralski-grown silicon at around 470°C and Koshka et al. [23] investigating multicrystalline edge-defined film-fed grown silicon by photoluminescence linking the 0.8 eV defect band to grain boundaries with accumulated impurities, such as oxygen.

To confirm the existence of oxygen clusters at sub-band-gap luminescence sites a transmission electron microscopy (TEM) sample is prepared out of the area of the solar cell where only sub-band-gap luminescence was detected. This area is marked by a yellow square in Fig. 1. The TEM sample was directly prepared at a cluster of the dendritic lines as showed in Fig. 1a). In the investigated area (100×100 μm^2) four precipitates were found. Fig. 3 exemplarily shows a TEM image of one of these precipitates and the corresponding EDX analysis spectra.

The spectrum shows a peak at 0.525 keV which is the oxygen Kα_1 peak. The EDX analysis at a reference point some hundred nm away from the precipitate shows no such oxygen peak. The EDX spectra of the other three precipitates show the same oxygen peak. At both positions no further EDX peaks are detected for energies up to 40 keV indicating that metal impurities do not contribute to the sub-band-gap luminescence.

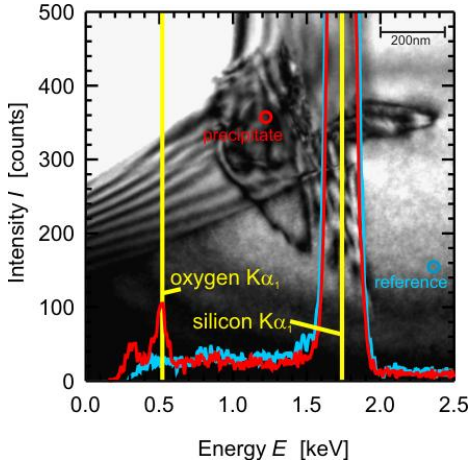

Figure 3: TEM image and EDX spectra of from center of the area marked by orange square in Fig. 1. This area is characterized by recombination at dendritic lines which also show strong sub-band-gap luminescence but no light emission under reverse bias. The EDX spectra taken of a precipitate located at the crossing point of two dislocation lines shows a clear oxygen Kα1 peak (yellow curve) while no oxygen is found at a reference point (blue curve) some microns away. Both regions show the characteristic silicon Kα1 peak.

For wafers with interstitial oxygen concentrations well above 2×10^{17} cm^{-3} as found in the bottom regions of mc-Si blocks, Möller et al. [24] reported that oxygen precipitation not only occurs at dislocations but also homogeneously throughout the bulk. Thus, solar cells made out of oxygen rich mc-Si wafers should show a homogeneous sub-band-gap luminescence emission superimposed by a stronger emission at dislocations sites. Investigating block-cast multicrystalline silicon solar cells from different block positions and oxygen concentrations, we are able to confirm this assumption experimentally. Figure 4 shows the sub-band-gap luminescence of two solar cells from different positions out of the same block. While solar cell a) from the bottom region of the block shows a homogeneous sub-band-gap emission superimposed by some brighter spots, cell b) from the middle region shows the typical bright local emission. It should be noted that solar cells from the very bottom region of a multicrystalline silicon block show a significantly reduced EL contrast compared to solar cells from the middle or top regions, independent of the interstitial oxygen concentration. Areas with characteristic dendritic lines or dark clusters resulting from twin boundaries accompanied by dislocations and stacking faults [25] are not frequently found in those cells. Since oxygen precipitation predominantly occurs at dislocation clusters, local sub-band-gap luminescence is more often found in solar cells coming from the middle or top regions of multicrystalline silicon blocks.

The light emission under reverse bias may follow from a perturbation of the electronic band structure which in general can be caused by both, metal impurities as well as oxygen-related defects. While a preference for SiO_x particles situated in the space charge region of the *p-n* junction has recently been published by Wagner and Weber [26], the incorporation of metal impurities cannot be excluded yet. Thus, from the current status we believe that sites contaminated with metal impurities appear in reverse-EL images, while clean oxygen precipitates at dislocation lines give rise to sub-band-gap luminescence.

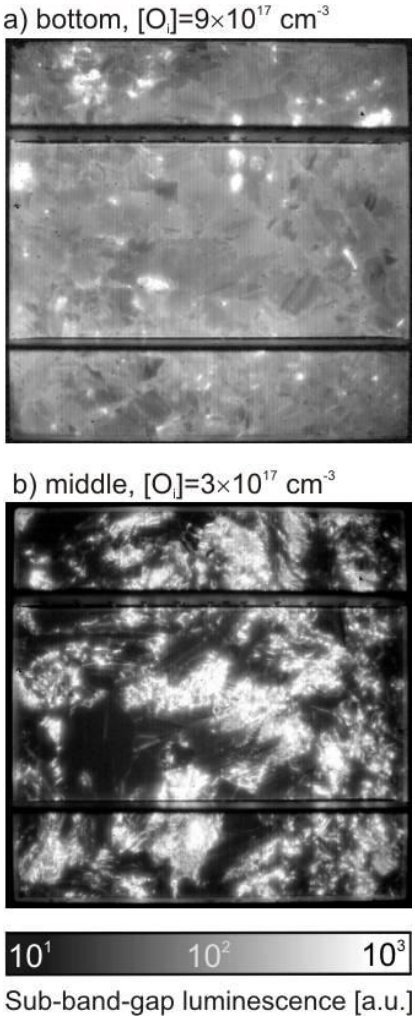

Figure 4: Integral sub-band-gap luminescence emission in the wavelength range between 1450 to 1700 nm detected from 0.6 V forward-biased block-cast multicrystalline silicon solar cells. The cells are taken from different block positions and with interstitial oxygen concentration of 9×10^{17} cm^3 at the bottom to 3×10^{17} cm^3 in the middle of the block. While cell a) taken from the bottom-near region shows a homogeneous luminescence emission superimposed by some bright spots, cell b) taken from the center region of the same block shows the characteristic local sub-band-gap luminescence emission.

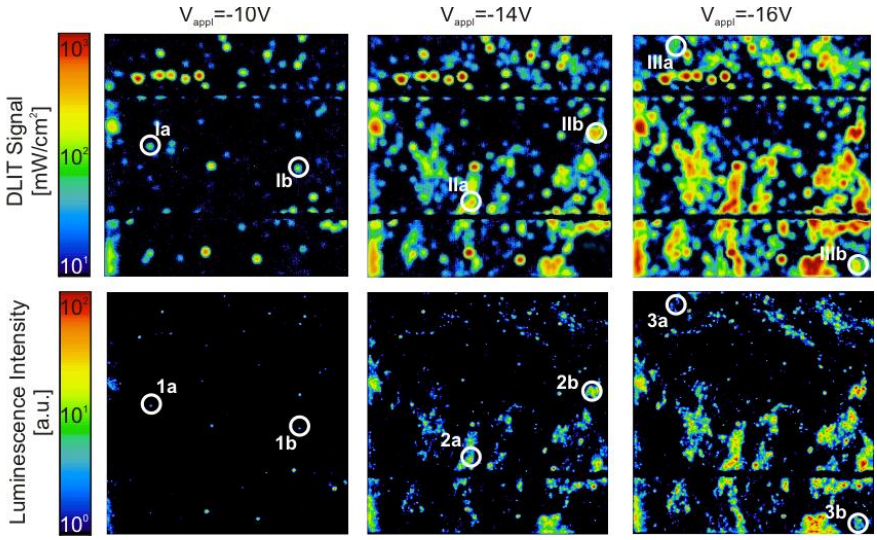

Figure 5: DLIT and EL images of a multicrystalline silicon solar cell at reverse-bias voltages ranging from -10 to -16 V. The positions marked with white circles are randomly chosen for detailed investigations of the local reverse characteristics (see Fig. 6).

The high current flow at local breakdown sites is associated with a local temperature increase. Thus, pre-breakdown sites under reverse bias can be well characterized by dark lock-in thermography (reverse-DLIT) [27]. However, the high spatial resolution of the luminescence images showing breakdown sites with diameters of some ten micrometers is masked in the DLIT measurements by the heat distribution around the individual spots. Figure 5 shows three DLIT images and three EL images of a multi-crystalline silicon solar cell for applied voltages ranging from -10 to -16 V. Comparing the two sets of images we find a very good correlation between the reverse-EL and reverse-DLIT signal since the emission of light is always accompanied by a temperature increase. This confirms the results of previous investigations [28].

For those spots marked by white circles in Fig. 5, Fig. 6 a) shows the complete reverse characteristic of the luminescence emission and Fig. 6 b) the characteristic of the DLIT signal given in absolute values of reverse current density. In order to allow for a direct comparison of sites with different absolute signal amplitudes, Fig. 6 c) shows luminescence as well as thermography data normalized to the signal measured at -20 V. The very good correspondence of the luminescence emission signal and the reverse current density shown in Fig. 6 c) indicates that the luminescence emission at one site depends linearly on the local current flow at that site. As summarized in Table I and discussed below, we distinguish between three different breakdown types detectable by both methods, reverse-EL and reverse-DLIT. Based on the analysis of reverse biased EL alone, a similar categorization was proposed previously [28,29].

As can be seen from Fig. 6 some sites (green curves) show a linear to super-linear breakdown characteristic with a well detectable heat and light emission at around -10 V while others (blue curves) show breakdown characteristics starting at reverse voltages above -12 V following a "soft" mono-exponential characteristic with an exponential pre-factor of 0.72±0.02. The thermal as well as the light emission of the latter sites tend to increase much more rapidly with increasing reverse voltage. Above -16 V sites (red curves) appear which show

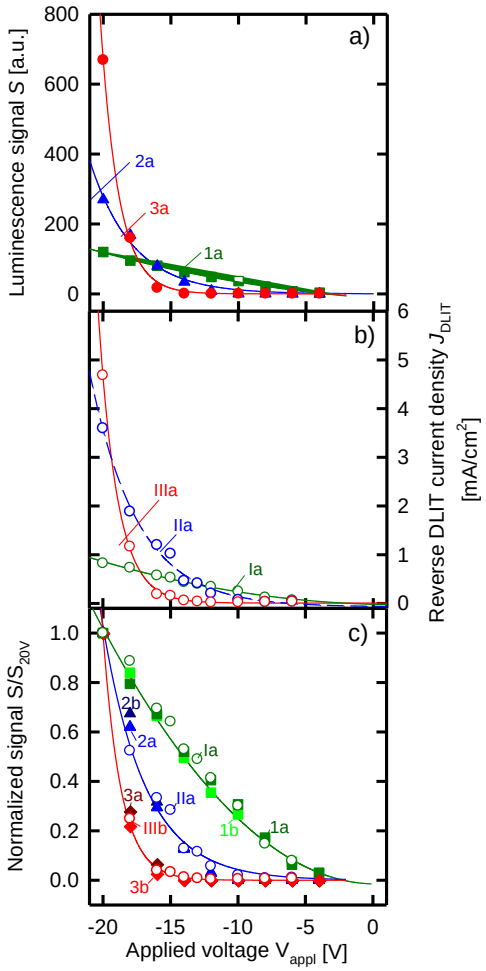

Figure 6: Local reverse characteristics of a) luminescence emission and b) DLIT current density for regions indicated by white circles in Fig. 5. Graph c) shows the data from a) and b) normalized to the signal measured at -20V. The excellent agreement of the luminescence and DLIT data indicates that the luminescence emission is proportional to the local current density.

Table I: Classification of the breakdown characteristics of block-cast multicrystalline silicon solar cells at room temperature and V_{appl}=-16V.

Breakdown characteristics	**Mechanism**	**Temperature coefficient of breakdown current**
linear, super-linear (green data set in Fig. 6)	probably internal field emission; tunneling assisted process via energy states in the band gap or in the vicinity of conductive channels	ambiguous around zero
soft exponential (blue data set in Fig. 6)	internal field emission with trap-assisted tunneling or trap-assisted avalanche, strong correlation with defect-rich areas showing a high recombination activity	slightly negative
hard exponential (red data set in Fig. 6)	avalanche breakdown due to high local electric fields (e.g. at thin emitter sites)	clearly negative

an extremely rapid increase of the light and thermal emission with increasing reverse voltage. From the analysis of a larger number of solar cells we know that the number of sites characterized by a "hard" mono-exponential characteristic with an exponential pre-factor of 0.31±0.02 is smaller compared to the number of all other pre-breakdown sites. As can be seen from the areas marked green in Fig. 1, this latter type of breakdown is only observed in regions of high EL intensity where no defect-related luminescence is detected.

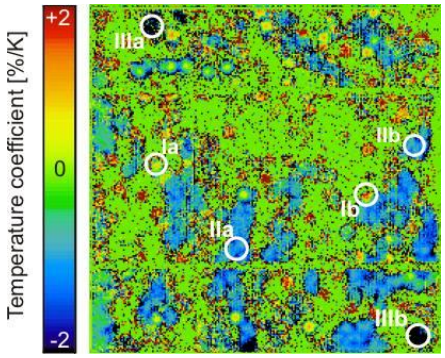

Figure 7: Image of the temperature coefficient TC of the breakdown current calculated from two DLIT images measured at an applied voltage of -16 V at 293 and 303 K, respectively. The temperature coefficient indicates the relative current change in percent per Kelvin temperature increase. The white circles indicate the same regions as in Fig. 5.

As has recently been proposed by Breitenstein et al. [30], images of the local temperature coefficient (TC) of the breakdown allow for a more detailed analysis of the underlying physical mechanism. Therefore, exemplarily Fig. 8 shows an image of the local temperature coefficient of the breakdown current calculated from two DLIT images measured at an applied voltage of -16 V and at 293 and 303 K, respectively. The temperature coefficient indicates the relative current change in percent per Kelvin temperature increase. The white circles indicate the same regions as in Fig. 6. Sites IIIa and IIIb, characterized by a hard-exponential breakdown characteristic, are found to have a clearly negative TC value of about -2. Investigating multicrystalline silicon solar cells from several different suppliers we have always found that those breakdown sites with a hard-exponential reverse characteristic show a negative TC as expected for avalanche breakdown. These results confirm first investigations by Wagner et al. [31] and more detailed investigations by Breitenstein et al. [30] and Bauer et al. [32].

With decreasing temperature the charge carriers can gain enough energy for avalanche breakdown since the number of phonons available for scattering decreases. Moreover, AB will only occur in areas of low crystallographic defect and impurity concentrations, since only in these regions the scattering probability is low enough for charge carriers to gain enough energy in the electric field. If additionally the electric field strength is locally enhanced, breakdown will occur preferentially at those sites. Such an enhancement occurs at etch pits where the junction tends to be thinner resulting in an increase of the local electric field strength. This effect has first been discussed by Shields [33] and by Senitzky and Moll [34] showing that avalanche breakdown occurs at lower voltages for junctions with smaller radii of curvature. More recently, first experimental results by Kasemann et al. [29] and a systematic study by Bauer et al. [32] provided clear experimental evidence that the strongly curved *p-n* junction at etch pits exhibits an electrostatic field strong enough to result in a local avalanche breakdown.

For those breakdown sites, showing a soft-exponential or linear to super-linear behaviour, it is more difficult to determine the temperature coefficient. While those sites showing a soft-exponential behaviour tend to have a slightly negative TC, sites showing a linear to super-linear behaviour tend to have a positive TC. The underlying physical mechanisms explaining the breakdown are not yet understood. Most likely a multi step field emission process can be hold responsible in both cases [25,31]. Depending on the type, density and nature of defects in the band gap, either a linear to super-linear or soft-exponential behavior is found. Crystallographic defects formed during the solidification process of multicrystalline silicon are often found to penetrate through several centimeters of the crystal along the direction of solidification. Therefore, especially in regions of high dislocation density conducting channels extending from the solar cells base region into the *p-n* junction should exist. Our results suggest that defect states in or in the vicinity of these channels support a multi-step field emission process.

3 CONCLUSIONS

The phenomenon of local junction breakdown in industrial multicrystalline silicon solar cells is investigated by camera-based dark lock-in thermography and electroluminescence imaging. The breakdown occurs locally at specific sites and is associated with an increase in temperature at those sites. For the majority of these sites the breakdown is associated with the emission of whitish light. This light is well detectable using a silicon CCD camera. Moreover an additional light emission is found in some areas to occur in the sub-band-gap range at wavelength between 1400 and 1700 nm. This emission occurs under forward bias and is due to defect-related radiative recombination of charge carriers. Even though there are areas where both effects, reverse-bias luminescence and sub-band-gap luminescence, are detected, we have not found a clear one-to-one correlation. We provide clear experimental evidence that oxygen plays a major role in the explanation of the defect-related sub-band-gap luminescence. This evidence results from EDX studies of precipitates at dislocations sites showing a clear Kα1 oxygen peak and the experimental finding that multicrystalline silicon solar cells with a high interstitial oxygen concentration for which bulk precipitation of oxygen is expected show a homogeneously distributed sub-band-gap luminescence signal.

However, more detailed studies on a larger number of cells are required in order to confirm the classification given above. From the finding that breakdown preferentially occurs at decorated crystallographic defects, we deduce the necessity for a careful analysis of multicrystalline silicon solar cells made from upgraded metallurgical-grade (UMG) silicon. Even though the efficiency of solar cells made from UMG silicon is basically not affected [35] by the higher impurity content of the feedstock material, these solar cells are known to suffer from considerably lower breakdown voltages. Studies on the microscopic level may result in a better understanding of the nature of the defects causing the local junction breakdown and the sub-band-gap luminescence, respectively. Once these mechanisms are understood, strategies for their avoidance might be deduced. Since the breakdown voltage limits the number of cells in the string of a solar module, a higher breakdown voltage would directly affect the module design allowing longer string lengths.

ACKNOWLEDGEMENT

Felix Dreckschmidt from the Technische Universität Bergakademie Freiberg is kindly acknowledged for providing sub-band-gap luminescence spectra.

REFERENCES

1. S. M. Sze and G. Gibbons, *Appl. Phys. Lett.* **8**, 111 (1966).
2. R. Newman, W.C. Dash, R.N. Hall, and W.E. Burch, *Phys. Rev.* **98**, 1536 (1955).
3. A. Goetzberger and W.Shockley, *Bull. Am. Phys. Soc.* **30**, 13 (1955).
4. R. Newman, *Phys. Rev.* **100**, 700 (1955).
5. R. Newman, W.C. Dash, R.N. Hall, and W.E. Burch, *Phys. Rev.* **98**, 1536 (1955)
6. A. Sio, S. Martinuzzi, *Proceedings of the 21st Photovoltaic Specialists Conference, Orlando* (IEEE, New York, 1990), p. 800.
7. J. W. Bishop, *Solar Cells* **26**, 335 (1989).
8. F. Dreckschmidt, T. Kaden, H. Fiedler, H.J. Möller, *Proceedings of the 22nd European Photovoltaic Solar Energy Conference, Milano, Italy* (WIP, Munich, 2007), p. 238.
9. O. Breitenstein, J. P. Rakotoniaina, and M. H. Al Rifai, Prog. Photovoltaics **11**, 515 (2003).
10. Y. Takahashi, Y. Kaji, A. Ogane, Y. Uraoka, and T. Fuyuki, *Proceedings of the Fourth World Conference on Photovoltaic Energy Conversion, Waikoloa, HI* (IEEE, New York, 2006), p. 924.
11. O. Breitenstein and M. Langenkamp, *Lock-in Thermography*, Springer Series in Advanced Microelectronics, Vol. 10 (Springer, Berlin, 2003).
12. S. D. Feldman, F. H. Seymour, T. R. Ohno, V. Kaydanov, and R. T. Collins, Mater. Res. Soc. Symp. Proc. **763**, B5.10.1 (2003).
13. K. Bothe, P. Pohl, J. Schmidt, T. Weber, P. Altermatt, B. Fischer, and R. Brendel, *Proceedings of the 21st European Photovoltaic Solar Energy Conference, Dresden, Germany* (WIP, Munich, 2006), p. 597.
14. K.G. McKay and A.G. Chynoweth, *Phys. Rev.* **99**, 1648 (1955).
15. A.G. Chynoweth and K.G. McKay, *Phys. Rev.* **102**, 369 (1956).
16. A.G. Chynoweth and K.G. McKay, *Phys. Rev.* **106**, 418 (1957).
17. H. Kressel, *RCA Review* **28**, 175 (1967).
18. S. Mahadevan, S. M. Hardas, G. Suryan, *Phys. Stat. Sol. (a)* **8**, 335 (1971).
19. R. Nitecki and B. Pohoryles, *Appl. Phys. A* **36**, 55 (1985).
20. Q. Li and R. W. Dutton, *IEEE Trans. Electron Devices* **38**, 936 (1991).
21. M. Kasemann, W. Kwapil, M. C. Schubert, H. Habenicht, B. Walter, M. The, S. Kontermann, S. Rein, O. Breitenstein, J. Bauer, A. Lotnyk, B. Michl, H. Nagel, A. Schütt, J. Carstensen, H. Föll, T. Trupke, Y. Augarten, H. Kampwerth, R. A. Bardos, S. Pingel, J. Berghold, W. Warta, S.W. Glunz, *Proceedings of the 33rd Photovoltaic Specialists Conference, San Diego* (IEEE, New York, 2008), DOI: 10.1109/PVSC.2008.4922478.
22. M. Tajima, *J. Crystal Growth* **103**, 1 (1990).
23. Y. Koshka, S. Ostapenko, I. Tarasov, S. McHugo, and J. P. Kaleys, *Appl. Phys. Lett.* **74**, 1555 (1999).
24. H.J. Möller, C. Funke, A. Lawerenz, S. Riedel and M. Werner, *Solar Energy Mater. Solar Cells* **72**, 403 (2002).
25. O. Breitenstein, J. Bauer, J.-M. Wagner, H. Blumtritt, A. Lotnyk, M. Kasemann, W. Kwapil, W. Warta, *Proceedings of the 34th Photovoltaic Specialists Conference, Philadelphia* (IEEE, New York, 2009), in press.
26. M. Wagner and T. Weber, *Proceedings of the 23nd European Photovoltaic Solar Energy Conference, Valencia, Spain* (WIP, Munich, 2008), p. 1338.
27. O. Breitenstein, J. Bauer, T. Trupke, R.A. Bardos, *Prog. Photovolt: Res. Appl.* **16**, 325 (2008).

28. W. Kwapil, M. Kasemann, J. Giesecke, B. Michl, and W. Warta, *Proceedings of the 23rd European Photovoltaic Solar Energy Conference, Valencia, Spain* (WIP, Munich, 2008), p. 1797.
29. M. Kasemann, W. Kwapil, B. Walter, J. Giesecke, B. Michl, M. The, J.-M. Wagner, J. Bauer, A. Schütt, J. Carstensen, S. Kluska, F. Granek, H. Kampwerth, P. Gundel, M.C. Schubert, R.A. Bardos, H. Föll, H. Nagel, P. Würfel, T. Trupke, O. Breitenstein, M. Hermle, W. Warta and S.W. Glunz, *Proceedings of the 23nd European Photovoltaic Solar Energy Conference, Valencia, Spain* (WIP, Munich, 2008), p. 965.
30. O. Breitenstein, J. Bauer, J.-M. Wagner and A. Lotnyk, *Prog. Photovolt: Res. Appl.* **16**, 679 (2008).
31. J.-M. Wagner, J. Bauer, A. Lotnyk, O. Breitenstein, *Proceedings of the 23nd European Photovoltaic Solar Energy Conference, Valencia, Spain* (WIP, Munich, 2008), p. 1164.
32. J. Bauer, J.-M. Wagner, A. Lotnyk, H. Blumtritt, B. Lim, J. Schmidt and O. Breitenstein, *Phys. Status Solidi RRL* **3**, 40 (2009).
33. J. Shields, *J. Electron. and Control* **4**, 58 (1958).
34. B. Senitzky and J. L. Moll, *Phys. Rev.* **110**, 612 - 620 (1958).
35. V. Hoffmann, K. Petter, J. Djordjevic-Reiss, E. Enebakk, J. T. Håkedal, R. Tronstad, T. Vlasenko, I. Buchovskaja, S. Beringov and M. Bauer, *Proceedings of the 23nd European Photovoltaic Solar Energy Conference, Valencia, Spain* (WIP, Munich, 2008), p. 1117.